International Journal of Chemical, Materials and Biomolecular Sciences
ISSN: 2415-6620
Vol:9, No:8, 2015

Mechanical and Chemical Properties of Zn-Ni-Al_2O_3 Nanocomposite Coatings

Soroor Ghaziof, Wei Gao

***Abstract*—**Zn alloy and composite coatings are widely used in buildings and structures, automobile and fasteners industries to protect steel component from corrosion. In this paper, Zn-Ni-Al_2O_3 nanocomposite coatings were electrodeposited on mild steel using a novel sol enhanced electroplating method. In this method, transparent Al_2O_3 sol was added into the acidic Zn-Ni bath to produced Zn-Ni-Al_2O_3 nanocomposite coatings. The effect of alumina sol on the electrodeposition process, and coating properties was investigated using cyclic voltammetry, XRD, ESEM and Tafel test. Results from XRD tests showed that the structure of all coatings was single γ-Ni_5Zn_{21} phase. Cyclic voltammetry results showed that the electrodeposition overpotential was lower in the presence of alumina sol in the bath, and caused the reduction potential of Zn-Ni to shift to more positive values. Zn-Ni-Al_2O_3 nanocomposite coatings produced more uniform and compact deposits, with fine grained microstructure when compared to Zn-Ni coatings. The corrosion resistance of Zn-Ni coatings was improved significantly by incorporation of alumina nanoparticles into the coatings.

***Keywords*—**Zn-Ni-Al_2O_3 composite coatings, steel, sol-enhanced electroplating, corrosion resistance.

I. Introduction

ZN alloy coatings are widely used in buildings and structures, automobile and fasteners industries. In recent years, Zn-Ni alloys have attracted much attention because of their higher corrosion resistance and better mechanical characteristics than pure Zn and other Zn based alloy coatings for steel components [1], [2]. However, demands for Zn-Ni coatings with better mechanical and corrosion properties are increasing for industrial applications. In order to meet the demands from industry, Zn-Ni based composite coatings have recently been developed to improve the mechanical and chemical properties [3], [4].

It is known that composite coatings produced by dispersing nano-sized particles in a coating matrix provide better mechanical properties and corrosion resistance [5]. Nanoparticles such as Al_2O_3, TiO_2 and ZrO_2 have been co-deposited with different metal and alloy coatings to produce composite coatings. This traditional process is using electrochemical deposition with nano-sized solid powder mixture into the electrolyte solution. The incorporation content and uniform dispersion of nanoparticles in the deposit are important factors that determine the properties and performance of the composite coatings. However, it is difficult to achieve good particle dispersion especially when they are in the nanometre scale due to very large surface area and surface energy. The nanoparticles tend to agglomerate together and deteriorate the desired properties [6], [7].

The current research applies a newly developed sol-enhanced method to prepare Zn-Ni-Al_2O_3 nanocomposite coatings. This method can avoid particle agglomeration by using solution mixing instead of adding solid powders, leading to true dispersed nanoparticle distribution [8], [9]. The technique combines sol-gel methods and traditional electroplating to prepare highly dispersed uniform oxide nanoparticle reinforced metal coatings. Based on this method, when a small amount of transparent sol was added into the electroplating solution, nanoparticles formed in-situ in the electrolyte and co-deposited into the coating matrix [10].

In the present work, attempts were made to produce Zn-Ni-Al_2O_3 composite coatings using a sol enhanced electrodeposition method. Surface morphology, microstructure and corrosion resistance of Zn-Ni-Al_2O_3 coatings were studied and compared to Zn-Ni alloy coating.

II. Materials and Experiments

A. Coatings and Sol Preparation

Zn-Ni alloy and Zn-Ni-Al_2O_3 composite coatings were electrodeposited from a sulfate acidic bath. The composition and electroplating parameters are summarized in Table I. All solutions were prepared with analytical grade reagents and distilled water. The pH of the bath was adjusted to 2 using a dilute H2SO4 solution. Mild steel sheet 1 mm in thickness was cut into 25×25 mm pieces and was used as the substrate. Nickel plates on both sides of the electroplating cell were used as anodes. Samples were prepared for coating by mechanically grounding with 600-grit SiC paper; followed by electropolishing in a solution of 95 vol.% acetic acid and 5 vol.% perchloric acid at 20 V for 3 min; and finally washing with distilled water.

For preparing the Al_2O_3 sol, 97% Al tri-sec-butoxide (ATSB) and distilled water were used in the mol ratio of 0.01:12.4. A small amount of absolute ethanol was added into the beaker to dissolve the ATSB. Under magnetic stirring, deionized water was slowly added into the mixture of ATSB and ethanol. Then 30% nitric acid was added into the solution to adjust the pH value to 3.5 and peptize the solution. At this stage, the solution contained white precipitates. This solution was stirred at 60°C until all white precipitates dissolved and clear sol was produced. 6 ml/l sol was added to the

S. Ghaziof is PhD Candidate at Department of Chemical and Materials Engineering, The University of Auckland, P.B 92019, Auckland 1142, New Zealand (corresponding author: phone No. +6493737599-ext. 88667 e-mail: sgha108@aucklanduni.ac.nz).

W. Gao is Professor at Department of Chemical and Materials Engineering, The University of Auckland, P.B 92019, Auckland 1142, New Zealand (e-mail: w.gao@auckland.ac.nz).

electrodeposition bath at 40oC to produce composite coating. The average size of the Al_2O_3 particles suspended in alumina sol used in the experiment as reinforcing phase is 10 nm which was measured with Malvern Zetasizer Nano Series Nano-ZS model instrument.

B. Coating Characterization

A field-emission scanning electron microscope was applied to analyze coating morphologies and cross-section. The phase structure of the coatings was determined using X-ray diffraction (XRD, D2 Phaser, BrukerAXS, Germany) with Cu Kα radiation at 30 kV and 10 mA. Diffraction patterns were recorded in the 2θ range from 20 to 90° at a step size of 0.02 °s−1 and scanning rate of 0.1 s/step. A MiniPal 2 PW4025 X-ray spectrometer (XRF) with Rhodium tube and spinner was also used for composition analysis. LA-ICP-MS test was applied to detect and measuring intensity of Al in composite coatings. A New Wave UP 213 laser with 213 nm wavelength coupled to a Perkin Elmer Elan DRCII ICP/MS spectrometer was used. 70% laser power used at 20 Hz frequency with 60 micron laser spot size. The scan was done on 2.5 mm line on surface of coatings with 20 µm/sec scan speed.

Microhardness of coatings was measured using a load of 100 g with a holding time of 15 s by using a Vickers hardness tester, and the average of ten hardness measurements was quoted as the hardness value.

The CV (Cyclic Voltammetry) experiments were initiated at -0.4 V vs. SCE in the negative direction, reversed at different switching potentials (-1.3 V to -1.5V) in a positive direction at a scan rate of 30 mV/s. A CHI 440 electrochemical workstation (CH instruments, USA) was used for CV test.

The corrosion resistance of the coatings was assessed by potentio-dynamic polarization curves measurements in 3.5 wt. % NaCl electrolyte using an electrochemical workstation. All corrosion tests were carried out at room temperature using a standard flat cell with three-electrode system, platinum mesh as auxiliary, Saturated Calomel Electrode (SCE) as reference and coated specimen as working electrode. The polarization curves were measured at a constant scan speed of 0.01 mV/s. The corrosion current density and corrosion potential were determined based on Tafel's extrapolation. The exposed surface area of all samples was 1 cm^2.

TABLE I
THE COMPOSITION OF ELECTROPLATING BATH AND PROCESSING PARAMETERS

Bath composition and processing parameters	Quantity
$ZnSO_4.7H_2O$	35 $g.L^{-1}$
$NiSO_4.6H_2O$	35 $g.L^{-1}$
$NaSO_4$	80 $g.L^{-1}$
Al_2O_3 sol (for composite coating)	6 $mL.L^{-1}$
Time	10 min
Current density	80 $mA.cm^{-2}$
Agitation speed	1200 rpm

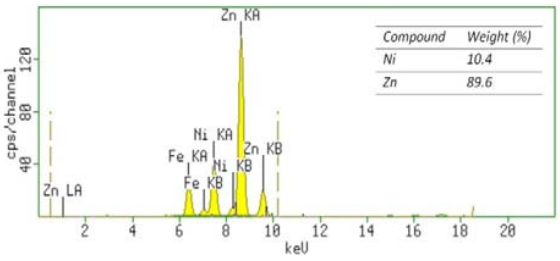

Fig. 1 XRF result for Zn-Ni coating. Electrodeposition parameters: temperature: 40°C, agitation speed: 600 rpm, current density: 80 mA/cm^2, time: 10 min

III. RESULTS AND DISCUSSION

A. Chemical Composition

Zn-Ni alloy coating and Zn-Ni-Al_2O_3 composite coatings were deposited on mild steel. The XRF results of coatings are summarized in Table II. All chemical composition values are quoted in weight percentage, representing the average of at least three measurements. Fig. 1 shows one of the XRF results as a sample. Fe peaks came from the steel substrate.

Results showed that the Ni content of Zn-Ni-Al_2O_3 composite coatings is slightly lower than that Zn-Ni. It means that incorporation of alumina into the Zn-Ni coating slightly decreased the Ni content in the coatings. Same results have been observed for Zn-Ni-TiO_2 and Zn-Ni-SiC composite coatings by co-deposition of TiO_2 and SiC particles [11], [12], [13]. This could be related to the promotion of hydrogen evolution reaction by composite particles on the Zn rich Zn-Ni electrodeposited films, favoring the formation of zinc hydroxide film on the electrode surface that hinders Ni2+ reduction [13].

It is worth mentioning that no Al peak was detected in XRF analysis of composite coatings. This was probably due to the extremely small particle size and relatively low oxide content, being below the detection limit of XRF. However, the results from LA-ICP-MS test on Zn-Ni-Al_2O_3 coatings showed the existence of Al compounds in the coatings. Fig. 2 shows the LA-ICP-MS test results of Al for Zn-Ni-Al_2O_3 composite coatings deposited at different agitation speed and also one Zn-Ni alloy coating without alumina for comparison. These LA-ICP-MS test results provide semi-quantitative results, indicating incorporation of alumina in the coatings. However, it was clear that no Al was detected for the pure Zn-Ni alloy.

TABLE II
XRF, MICROHARDNESS AND CORROSION TEST RESULTS OF ZN-NI COATING AND ZN-NI-AL2O3 COMPOSITE COATINGS

coating	Ni Content (wt%)	Microhardness (Hv_{100})	$E_{corr.}$ Vs. SCE (mV)	icorr. ($\mu A/cm^2$)
Zn-Ni	10.4 ± 0.1	237± 7	-1048	6
Zn-Ni-Al_2O_3	10.0 ± 0.1	312± 13	-1013	0.8

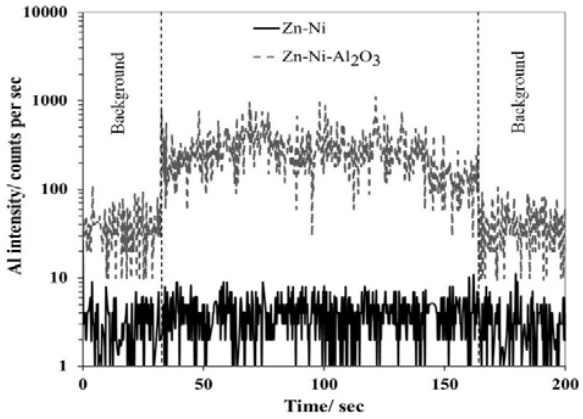

Fig. 2 LA-ICP-MS results of Al for Zn-Ni-Al_2O_3 coatings. Analysis from Zn-Ni alloy is also shown for comparison

B. Cyclic Voltammetry (CV) Studies

Fig. 3 shows a CV test on the mild steel electrode in a bath solution with and without alumina sol. A broad peak was observed for each cathodic scan at potentials from ~ -0.72 to -1.10 V vs. SCE (peak A). This peak is related to the hydrogen evolution reaction on the cathode surface [14], [15], which was also observed directly during the test. Within this potential range, the current density increased gradually, reached a maximum, and then decreased. The reduction of Zn-Ni deposits (peak B) was started at ~ -1.1 V vs. SCE. The presence of alumina sol had little effect on the hydrogen evolution current density (peak A) when compared to a Zn-Ni bath without sol. However, alumina nanoparticles in the bath have slightly affected the electrodeposition overpotential, which was a little lower in the presence of alumina sol in the bath, and caused the reduction potential of Zn-Ni to shift to more positive values. The shift in reduction potential was attributed to an increase in the active surface area due to the adsorbed particles on the cathode and to a possible increase in ionic transport by nanoparticles with their ionic layers adsorbed [16].

The anodic sweep exhibits two distinct dissolution peaks for the Zn-Ni alloy and Zn-Ni-Al_2O_3 composite coatings. The first peak (peak C), centered at about -0.89 V vs. SCE is due to Zn dissolution from the η phase [17] (a solid solution of Ni in Zn with hexagonal structure, containing up to 1 wt% Ni), and the second peak (peak D), centered at -0.65 V vs. SCE is related to dissolution of the γ phase [17] (an intermetallic compound Ni_5Zn_{21} with a bcc structure). Beyond this peak the current approached zero, indicating that the majority of the deposited coatings had been removed from the substrate surface.

It is worth mentioning that dissolution of mild steel substrate has occurred at the potentials greater than ~ -0.5 V vs. SCE (peak E). Fig. 1 also depicts the results of a blank test performed in an aqueous solution containing only Na_2SO_4 without metal ions, which exhibited no peaks except peak E which is related to dissolution of the steel substrate.

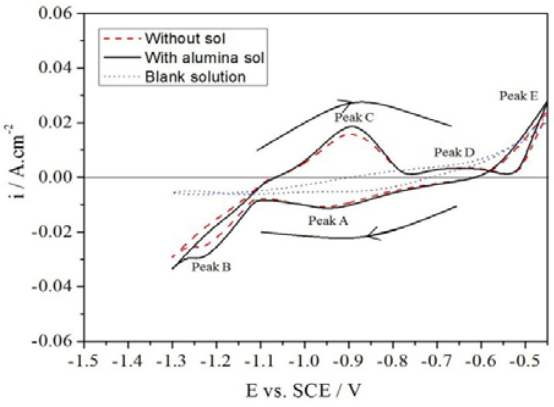

Fig. 3 CV tests on the mild steel electrode in the electroplating bath solution with and without alumina sol and also in the bath solution without metal ions (Blank solution) Scan rate 30 mV/s, T = 40°C, pH 2

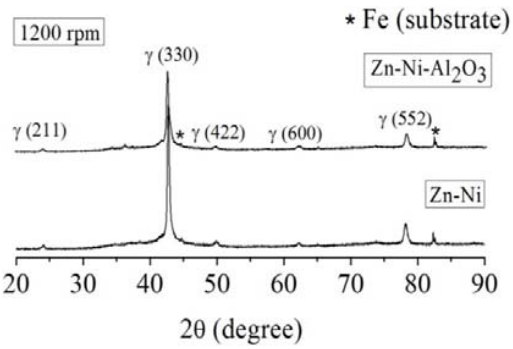

Fig. 4 XRD results for Zn-Ni and Zn-Ni-Al_2O_3 coatings

C. Phase Structure

Fig. 4 shows the XRD pattern of Zn-Ni alloy and Zn-Ni-Al_2O_3 composite coatings. It can be seen that the phase structure of all of deposits is single γ-Ni_5Zn_{21} phase which is the desirable phase structure for Zn-Ni coatings. It has been reported that Zn-Ni coatings of single γ-Ni_5Zn_{21} phase structure with Ni content in the range of 10-14 wt.% has shown five times better corrosion resistant compared to pure Zn [1], [2].

Grain size measurement was conducted based on the Scherrer line broadening equation, which is well suited to detect grain size smaller than 100 nm, and have been used widely for Zn-Ni deposits [2], [18]. The grain size, D, was calculated from broadening of the most intensive peak (330) using the Scherrer equation, $D = 0.9\,\lambda/\beta\cos\theta$, where λ is the wavelength of the radiation (0.154 nm), β is the full width at half-maximum (FWHM) of the peak, and θ is the position of the peak. The grain size of Zn-Ni and Zn-Ni-Al_2O_3 coatings were 30±0.1 and 23±0.2 nm, respectively, indicating that the composite coatings have smaller grain size than alloy coatings. Therefore, incorporation of Al_2O_3 nanoparticles in the coating refined the crystals. It should be noted that all coatings' grain sizes are in the nanometer scale, confirming the nanocrystalline structure of Zn-Ni and Zn-Ni-Al2O3 composite coatings.

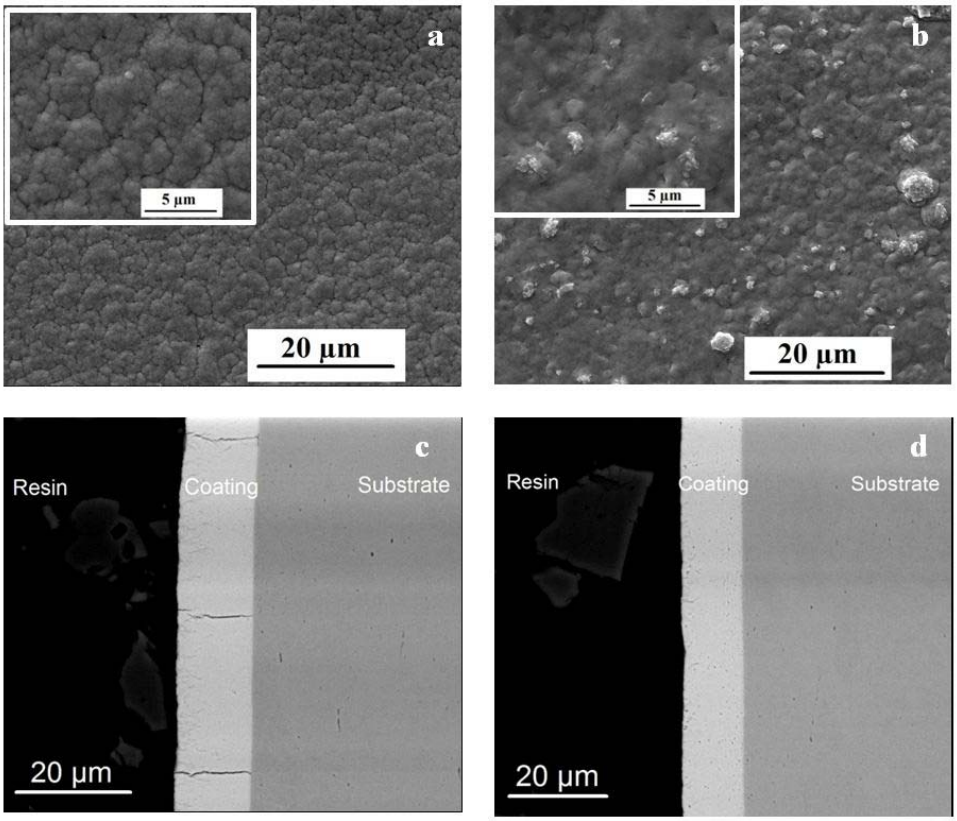

Fig. 5 ESEM images of a) Zn-Ni coating, b) Zn-Ni-Al_2O_3 coating, and cross-section images of c) Zn-Ni coating d) Zn-Ni-Al_2O_3 coating

D.Surface Morphology and Cross-Section Images

Fig. 5 shows the surface morphology and cross-section images of Zn-Ni and sol enhanced Zn-Ni-Al_2O_3 coatings. As can be seen in Fig. 5 (a), Zn-Ni coatings showed relatively homogeneous hemispherical nodules with average size of 6 µm. However, surface morphology of sol enhanced Zn-Ni-Al_2O_3 composite coatings (Fig. 5 (b)) was completely different from alloy coatings. Zn-Ni- Al_2O_3 coating showed smoother nodular background containing some areas with "cauliflower-like" morphology. Cross-section images of coatings (Figs. 5 (c) and (d)) showed that Zn-Ni alloy coatings deposited consisted of through-thickness microcracks (Fig. 5 (c)). However, composite coatings (Fig. 5 (d)) showed cracked-free cross section images. Therefore, it can be concluded that Zn-Ni-Al2O3 composite coatings provided more compact and crack-free deposit compared to Zn-Ni alloy coatings.

E. Mechanical and Corrosion Properties

The microhardness results of Zn-Ni alloy and Zn-Ni- Al_2O_3 composite coatings electroplated at different agitation speeds are summarized in Table II. The results indicated that Zn-Ni-Al_2O_3 composite coatings showed higher microhardness compared to Zn-Ni alloy coatings. The variation of microhardness results can be attributed to the incorporation of Al_2O_3 nanoparticles, Ni content and microstructure changes. As mentioned previously, the Ni content did not change significantly for composite and alloy coatings. Therefore, the increase in microhardness of the composite coatings should be mainly came from the matrix grain refinement (refer to XRD results) and dispersion strengthening because of incorporation of hard alumina nanoparticles into the Zn-Ni alloy coating. Dispersion strengthening is associated with the incorporation of fine particles (< 1 µm) and is the result of hindered dislocation motion of matrix by fine particles. In grain refining, the structural refinement is resulted from the nucleation of small grains on the surface of the incorporated particles. The high density of grain boundaries impedes dislocation motion, resulting in increased microhardness [19].

Tafel tests were performed on Zn-Ni alloy and Zn-Ni-Al_2O_3 composite coatings in 3.5 % NaCl solution. Tafel polarization readings have been shown in Fig 6. The corresponding electrochemical parameters extracted from Tafel plots are summarized in Table II. Results indicated that the corrosion potentials of Zn-Ni-Al_2O_3 composite coatings shift to the positive direction and corrosion current density decreased significantly compared to Zn-Ni alloy coatings. The reason could be because of incorporation of Al_2O_3 nanoparticles in the coatings. Researches have shown that incorporation of non-metallic particles has improved the corrosion performance of Zn-Ni coatings [3], [5], [20]. Some researchers related this to the fact that the embedded inert oxide/carbide particles diminish the active surface in contact with the corrosive environment. In addition, they believe that the metal surface possess defects, gaps, crevices and holes

which were usually larger than micron in sizes. Inserted nanoparticles in the coating may fill these defects, slowing down the dissolution of metal through these active sites [21], [22].

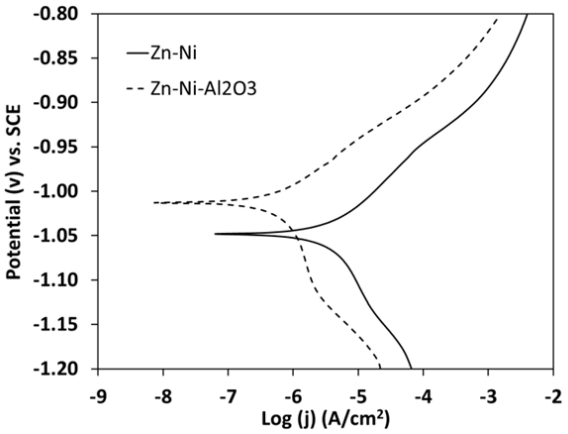

Fig. 6 Polarization curves of the Zn-Ni alloy and Zn-Ni-Al2O3 composite coatings on the steel substrate in 3.5 wt. % NaCl solution

ACKNOWLEDGMENT

This work is partially supported by a New Zealand Marsden project and NPRP Grant NPRP-4-662-2-249 from the Qatar National Research Fund (a member of Qatar Foundation). The authors would like to thank the technical staff in the Department of Chemical and Materials Engineering, the University of Auckland for their various assistances.

REFERENCES

[1] Boonyongmaneerat Y, Saenapitak S, Saengkiettiyut K. Reverse pulse electrodeposition of Zn–Ni alloys from a chloride bath. J Alloys Compounds. 2009 11/13;487(1–2):479-82.
[2] Abou-Krisha MM. Effect of pH and current density on the electrodeposition of Zn–Ni–Fe alloys from a sulfate bath. Journal of Coatings Technology and Research:1-9.
[3] Blejan D, Bogdan D, Pop M, Pop AV, Muresan LM. Structure, morphology and corrosion resistance of Zn-Ni-TiO2 composite coatings. Optoelectronics and Advanced Materials, Rapid Communications. 2011;5(1):25-9.
[4] Zheng H, An M. Electrodeposition of Zn–Ni–Al2O3 nanocomposite coatings under ultrasound conditions. J Alloys Compounds. 2008 7/14;459(1–2):548-52.
[5] B.M. Praveen1 and T. V. Venkatesha2. Electrodeposition and Corrosion Resistance Properties of Zn-Ni/TiO2 Nano composite Coatings. International Journal of Electrochemistry. 2011;2011.
[6] Wang W, Hou F, Wang H, Guo H. Fabrication and characterization of Ni–ZrO2 composite nano-coatings by pulse electrodeposition. Scr Mater. 2005;53(5):613-8.
[7] Oberle R, Scanlon M, Cammarata R, Searson P. Processing and hardness of electrodeposited Ni/Al2O3 nanocomposites. Appl Phys Lett. 1995;66(1):19-21.
[8] Yang Y, Chen W, Zhou C, Xu H, Gao W. Fabrication and characterization of electroless Ni–P–ZrO2 nano-composite coatings. Appl Nanosci. 2011 2011/05/01;1(1):19-26.
[9] Chen W, He Y, Gao W. Electrodeposition of sol-enhanced nanostructured Ni-TiO2 composite coatings. Surface and Coatings Technology. 2010 4/25;204(15):2487-92.
[10] Chen W, He Y, Gao W. Synthesis of Nanostructured Ni–TiO2 Composite Coatings by Sol-Enhanced Electroplating. J Electrochem Soc. 2010;157(8):E122-8.
[11] Gomes A, Almeida I, Frade T, Tavares AC. Stability of Zn-Ni-TiO 2 and Zn-TiO 2 nanocomposite coatings in near-neutral sulphate solutions. Journal of Nanoparticle Research. 2012;14(2).
[12] Gomes A, Almeida I, Frade T, Tavares AC. Zn-TiO 2 and ZnNi-TiO 2 nanocomposite coatings: Corrosion behaviour; 2010 (cited 17 September 2012).
[13] Tulio PC, Rodrigues SEB, Carlos IA. The influence of SiC and Al2O3 micrometric particles on the electrodeposition of ZnNi films and the obtainment of ZnNi–SiC and ZnNi–Al2O3 electrocomposite coatings from slightly acidic solutions. Surface and Coatings Technology. 2007 11/15;202(1):91-9.
[14] Casanova T, Soto F, Eyraud M, Crousier J. Hydrogen absorption during zinc plating on steel. Corros Sci. 1997 3;39(3):529-37.
[15] Abou-Krisha M, Assaf F, Toghan A. Electrodeposition of Zn–Ni alloys from sulfate bath. Journal of Solid State Electrochemistry. 2007;11(2):244-52.
[16] Benea L, Bonora PL, Borello A, Martelli S, Wenger F, Ponthiaux P, et al. Composite electrodeposition to obtain nanostructured coatings. J Electrochem Soc. 2001;148(7):C461-5.
[17] Hegde AC, Venkatakrishna K, Eliaz N. Electrodeposition of Zn–Ni, Zn–Fe and Zn–Ni–Fe alloys. Surface and Coatings Technology. 2010 12/25;205(7):2031-41.
[18] Elkhatabi F, Benballa M, Sarret M, Müller C. Dependence of coating characteristics on deposition potential for electrodeposited Zn–Ni alloys. Electrochim Acta. 1999 1;44(10):1645-53.
[19] Damjanovic A, Setty T, Bockris J. Effect of Crystal Plane on the Mechanism and the Kinetics of Copper Electrocrystallization. J Electrochem Soc. 1966;113(5):429-40.
[20] praveen BM, Venkatesha TV. Electrodeposition and properties of Zn–Ni–CNT composite coatings. J Alloys Compounds. 2009 8/12;482(1–2):53-7.
[21] Praveen BM, Venkatesha TV. Electrodeposition and properties of Zn-nanosized TiO2 composite coatings. Appl Surf Sci. 2008 2/15;254(8):2418-24.
[22] Praveen BM, Venkatesha TV, Naik YA, Prashantha K. Corrosion behavior of Zn-TiO2 composite coating. Synthesis and Reactivity in Inorganic, Metal-Organic and Nano-Metal Chemistry. 2007;37(6):461-5.